NUCLEUS-NUCLEUS COLLISIONS AT INTERMEDIATE AND RELATIVISTIC ENERGIES*,**

P. DANIELEWICZ

National Superconducting Cyclotron Laboratory
and
Department of Physics and Astronomy
Michigan State University
East Lansing, Michigan 48824, USA

(Received August 28, 1993)

Physics aspects of the energetic heavy-ion reactions, including changes in the bulk properties of matter during reactions and features of transport description, are discussed. Observables such as particle correlations, mean momentum in the reaction plane, light-fragment yields and spectra are reviewed, together with the information these observables provide on size of the emission region, magnitude of nuclear compressibility, production of entropy, and energy of collective expansion.

PACS numbers: 25.75. +r, 21.65. +f, 25.70. Pq

1. Introduction

In energetic reactions the nuclei are broken up into nucleons and lighter nuclei. High-energy gamma rays are produced and possibly π, K, or η mesons, or lepton pairs. The important objective of the reaction studies is to assess, from the products, the properties of nuclear matter that is highly excited and compressed in reactions. Of interest is whether various particles and their interactions are modified in the matter compared to the vacuum.

The reaction measurements are carried out at the synchrotrons SIS at GSI and SATURNE at Saclay delivering beams of energy of 2 GeV/nucleon and 1.15 GeV/nucleon, respectively, for projectiles with $Z/A = 0.5$.

---

* Presented at the XXIII Mazurian Lakes Summer School on Nuclear Physics, Piaski, Poland, August 18–28, 1993.

** This work was partially supported by the National Science Foundation under Grant Nos. PHY90-17077 and PHY89-04035.

The Synchrophasotron at Dubna can supply beams with energy up to 4 GeV/nucleon, however of low intensity. Data from the shut-down Bevalac have been recorded on tapes and are going to be analysed in the next couple of years. The cyclotrons K1200 at MSU and GANIL at Caen supply beams of energy up to 180 MeV/nucleon and 95 MeV/nucleon, respectively, for the symmetric projectiles.

Reaction process is generally quite complex. A proper theoretic description may need to account for a variety of physical effects such as motion of nucleons in a self-consistent optical potential, Coulomb effects, nucleon–nucleon scattering, finite interaction-range effects, Pauli principle, and inelasticity in elementary processes. The uncertainties associated with each of these effects generally hamper the isolation of specific information from collisions. Proper robust observables must be used in comparing the results of measurements and calculations. In the following, I shall discuss the changes in the bulk properties of matter in collision and further the transport descriptions of collisions. Subsequently I shall turn to the comparisons between data and calculations and to the extracted information.

2. Nuclear matter in collision

Figure 1 shows the energy per nucleon in nuclear matter as a function of the nucleon density.

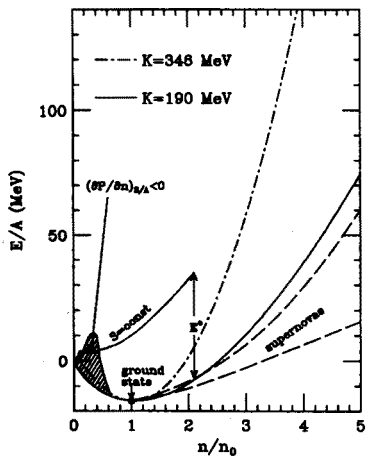

Fig. 1. Energy per nucleon of nuclear matter as a function of density.

The nuclei in their ground state correspond to the minimum of this energy. Parabolic curves indicate possible behavior of the energy in cold matter with variation of density. The parameter quantifying stiffness of cold matter is

the compressibility constant K, first introduced to characterize the behavior of energy with nuclear radius,

$$K = R^2 \frac{d^2}{dR^2} \frac{E}{A} = 9\, n_0^2 \frac{d^2}{dn^2} \frac{E}{A}. \tag{1}$$

In the collisions the matter is not only compressed but also excited to an energy higher than at zero temperature, by E^*, see Fig. 1. Aside from the collisions, the compression of nuclear matter takes place in the collapse of massive stars such as leading to the supernova explosions and formation of neutron stars. In the neutron stars nuclear matter remains at a low excitation energy E^*, with a high isospin asymmetry. In the collisions, following the compression and excitation, matter expands into vacuum, in a fashion that is most likely isentropic till the freezeout. If the initial entropy is low, $S/A \lesssim 3$, or otherwise E^* is low, the expanding system crosses the region of a phase transition at densities lower than normal. Of a potential importance for the dynamics are the growth factors [1] for modes that are unstable when $(\partial P/\partial n)_{S/A} < 0$ in this region. For the entropies close to 3 (system entering instability region from the left of the critical point) these factors are low, and thus system may shoot through the region without taking notice of the instability. For $S/A \sim 2$ the growth factors are high and system may undergo a violent fragmentation. For lower entropies the system may recontract and decay through evaporation.

3. Transport description of collisions

First microscopic model introduced to describe the energetic reactions of medium and heavy nuclei was the cascade model [2, 3]. In the model the initial nuclei are treated as a loose collection of nucleons. During the reaction the nucleons collide with the free differential cross sections at higher relative energies, $d\sigma_{NN}/d\Omega$. Nucleon statistics is ignored. The production of π mesons is described as a two-step process. First a nucleon is excited to a Δ resonance. Then the resonance decays into a nucleon and a pion. This model has been successful in describing the inclusive proton spectra at the high energies, but not so at the intermediate energies, see Fig. 2.

The description of the spectra at lower energies in the reactions, Fig. 2, and of the some more sophisticated observables at higher energies, considerably improved upon taking into account the effects of Pauli principle and of nucleon average-potential in the model [7, 8] based on a Boltzmann equation for the nucleon occupation-function f,

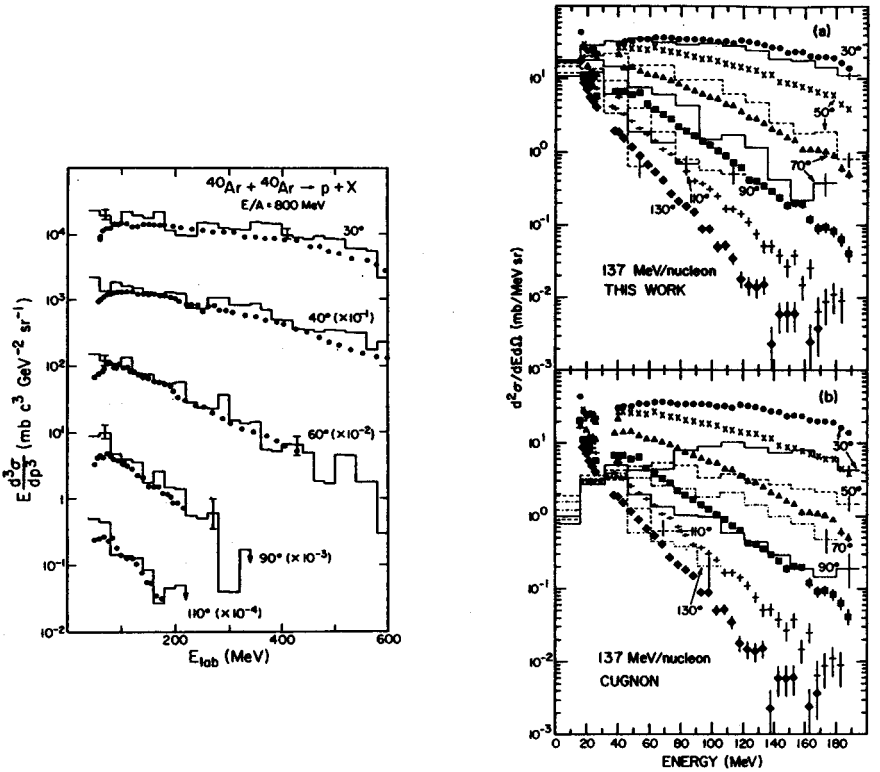

Fig. 2. Inclusive proton spectra measured in the reactions Ar + KCl at 800 MeV/nucleon [4] and Ar + Ca at 137 MeV/nucleon [5], compared to the spectra calculated within the extended transport model [6] (panel marked THIS WORK) and within the cascade model [3] (remaining panels). Data are indicated with points, and calculations with histograms.

$$\frac{\partial f}{\partial T} + \frac{\partial \epsilon_{\mathbf{p}}}{\partial \boldsymbol{p}} \frac{\partial f}{\partial \boldsymbol{R}} - \frac{\partial \epsilon_{\mathbf{p}}}{\partial \boldsymbol{R}} \frac{\partial f}{\partial \boldsymbol{p}}$$
$$= \frac{1}{m^2 \pi^3} \int d\boldsymbol{p}_1 d\boldsymbol{p}' d\boldsymbol{p}'_1 \delta(\boldsymbol{p} + \boldsymbol{p}_1 - \boldsymbol{p}' - \boldsymbol{p}'_1) \delta(\epsilon_{\mathbf{p}} + \epsilon_{\mathbf{p}_1} - \epsilon_{\mathbf{p}'} - \epsilon_{\mathbf{p}'_1})$$
$$\times \frac{d\sigma_{NN}}{d\Omega} \left((1-f)(1-f_1) f' f'_1 - f f_1 (1-f')(1-f'_1) \right) . \qquad (2)$$

Here $\epsilon_{\mathbf{p}}$ is single-particle energy, $\partial \epsilon_{\mathbf{p}} / \partial \boldsymbol{p}$ is velocity, and $-\partial \epsilon_{\mathbf{p}} / \partial \boldsymbol{R}$ is force. The r.h.s. of the equation describes the changes in the occupation function due to NN collisions. The second and third term on the l.h.s. describe the changes due to the motion within an average potential field. The occupation

function is related to spatial density by

$$n = \frac{4}{(2\pi)^3} \int dp\, f\,.$$

The single-particle energies in the model [8] are parametrized by regarding the total energy as a functional of the distribution function,

$$\epsilon_{\mathrm{p}}(r) = \frac{(2\pi)^3}{4} \frac{\delta E}{\delta f(p,r)} = \frac{(2\pi)^3}{4} \frac{\delta}{\delta f(p,r)} \left(E^{\mathrm{kin}} + E^{\mathrm{pot}}\right) = \epsilon_{\mathrm{p}}^{\mathrm{kin}} + V(p,r)\,, \tag{3}$$

with V — the potential. The potential energy may be taken in the form

$$E_{\mathrm{pot}} \simeq \int dr n \left[\frac{A}{2}\frac{n}{n_0} + \frac{B}{\gamma+1}\left(\frac{n}{n_0}\right)^{\gamma} + \frac{C}{n_0}\frac{4}{(2\pi)^3}\int dp \frac{f}{1+p^2/\Lambda^2} + D\nabla^2 n\right] + E_{\mathrm{coul}}\,, \tag{4}$$

with constants adjusted so that the energy per nucleon in nuclear matter has a proper minimum, and that nuclear surface profiles are adequately reproduced within the Thomas–Fermi approximation. The parametrization leaves flexibility with regard to the values of compressibility K and effective mass $m^* = p(\partial\epsilon_p/\partial p)^{-1}$. The potential becomes

$$V = A\frac{n}{n_0} + B\left(\frac{n}{n_0}\right)^{\gamma} + \frac{C}{n_0}\frac{4}{(2\pi)^3}\int dp \frac{f}{1+p^2/\Lambda^2} + C\frac{n}{n_0}\frac{1}{1+p^2/\Lambda^2} + 2D\nabla^2 n + V_{\mathrm{coul}}\,. \tag{5}$$

4. Intensity interferometry

The proton spectra probe the process of dissipation of the longitudinal motion in the reactions. Space-time dimensions of the emission zone at freezeout may be accessed through the intensity interference.

This technique relies on the fact that the probability for registering two particles with a low relative velocity is different from the product of probabilities for the individual particles. At high energies identical pions are used and deviations from the product of probabilities are due to Bose interference. For nuclear fragments the primary role is played by a mutual interaction of particles moving toward the detectors. If differences between

particle emission times can be ignored, the ratio of probability densities, or correlation function, for particles with momenta $\boldsymbol{p}_1$ and $\boldsymbol{p}_2$

$$C(\boldsymbol{p}_1, \boldsymbol{p}_2) = \frac{\sigma \frac{d\sigma}{d\boldsymbol{p}_1 d\boldsymbol{p}_2}}{\frac{d\sigma}{d\boldsymbol{p}_1}\frac{d\sigma}{d\boldsymbol{p}_2}}, \tag{6}$$

may be expressed as [9]

$$C(\boldsymbol{p}_1, \boldsymbol{p}_2) \simeq \int d\boldsymbol{r}_1 \int d\boldsymbol{r}_2 S(\boldsymbol{r}_1, \boldsymbol{p}_1, \boldsymbol{r}_2, \boldsymbol{p}_2) \left|\Psi_{\boldsymbol{p}_1\boldsymbol{p}_2}(\boldsymbol{r}_1, \boldsymbol{r}_2)\right|^2 . \tag{7}$$

In this expression of a DWBA-type, Ψ is a 2-particle wavefunction and S is a normalized source. The correlation between particles is generally pronounced for compact sources, and it is weak for extended sources. Furthermore, differences in emission times effectively increase the source size.

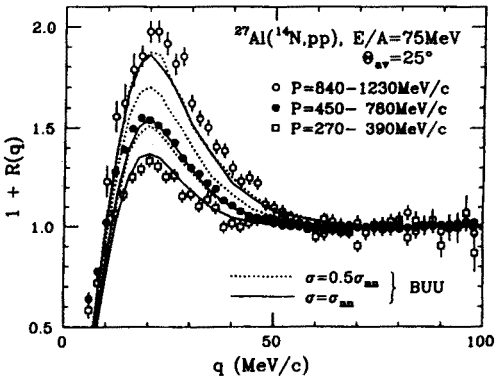

Fig. 3. Two-proton correlation functions, measured for the reaction ^{14}N + ^{27}Al at 75 MeV/nucleon (points), compared with correlation functions from transport theory (lines), after [10]. The gates placed on the total momenta P of the coincident particle pair are indicated.

Fig. 3 shows the $p - p$ correlation function measured in the reaction N + Al at 75 MeV/nucleon. High-energy protons appear to be emitted from a more compact source than low-energy protons. This feature is reproduced in the calculation using emission points from a model based on Eq. (4).

5. Reaction dynamics

Similar consistency between the results of measurements and calculations to that for the shown proton spectra and correlation functions, is found

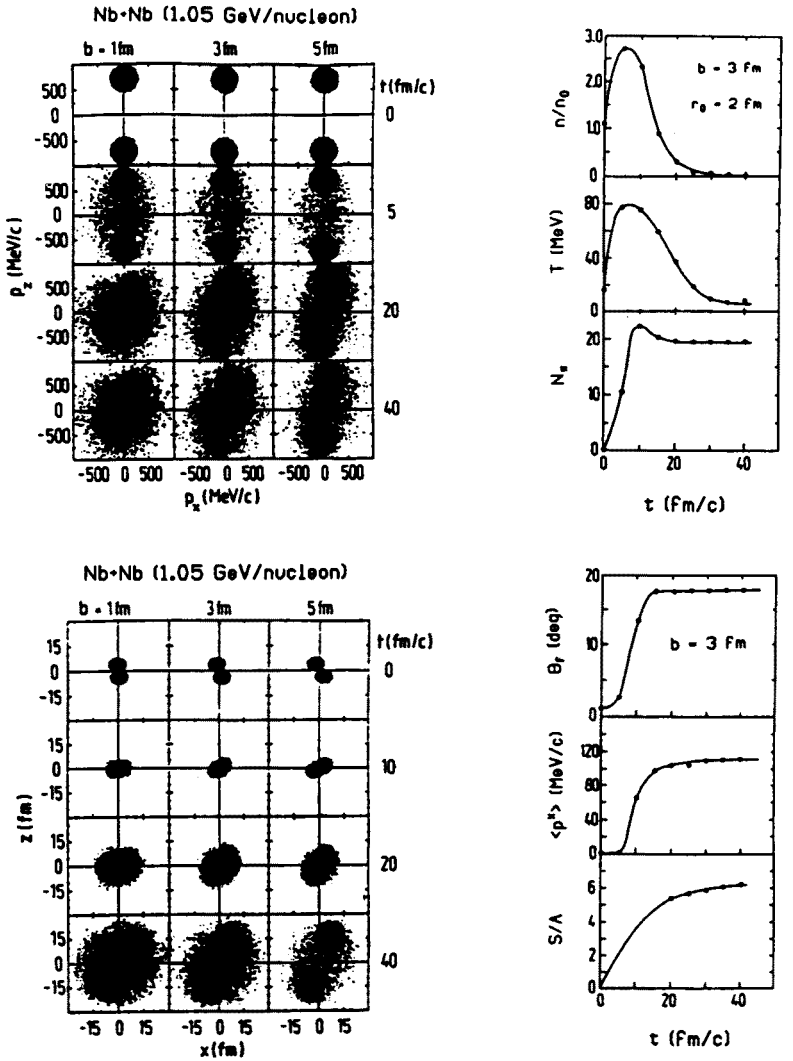

Fig. 4. Time evolution of the single-particle distributions in configuration and momentum space and of a few variables in the Nb + Nb reaction at 1.05 GeV/nucleon [11].

for some other observables from energetic collisions. This makes plausible the history of the collisions within the transport model.

Fig. 4 shows the evolution of nucleon distribution in configuration space and momentum space and of a few variables in the Nb + Nb reaction at 1.05 GeV/nucleon [11]. It is seen that during the compression stage at this energy, the densities in excess of $2.5n_0$ are reached in the central region.

Although it is arguable whether the equilibrium is reached, the authors chose to characterize the system in terms of temperature, finding T close to 80 MeV during compression. Most pions and most entropy are produced during the initial period. The entropy may be accessed experimentally by studying particle yields.

If the system were equilibrated and away from degeneracy,

$$f \simeq \exp\left(\frac{\mu - \epsilon_p}{T}\right),$$

the entropy could be expressed in terms of the ratio of the nucleon chemical potential μ to temperature

$$S = -\frac{4}{(2\pi)^3}\int d\boldsymbol{r}d\boldsymbol{p}\,(f\log f + (1-f)\log(1-f)) \simeq A\left(\frac{5}{2} - \frac{\mu}{T}\right). \quad (8)$$

The ratio in turn is related to the ratio of deuterons (chemical potential 2μ) to protons, and other particle ratios,

$$\frac{N_d}{N_p} \propto \frac{\exp\left(\frac{2\mu}{T}\right)}{\exp\left(\frac{\mu}{T}\right)}. \quad (9)$$

The entropy per nucleon may be expressed finally as

$$\frac{S}{A} \simeq 3.9 - \log\frac{N_d}{N_p}. \quad (10)$$

It may be argued that such relations as (10) should be also valid outside of equilibrium [12]. Entropy deduced from the measured particle ratios [13] is lower than that found in the calculation [11].

Concerning collisions where low values of entropy are generated, it should be noted that a model based solely on Eq. (2) is not capable of properly describing the fragmentation.

6. Determination of nuclear compressibility

Some recent attempts to determine the nuclear compressibility in the collisions relied on the sideward deflection of forward- and backward-moving particles in the c.m. system, such as seen in Fig. 4. This deflection may be quantified by evaluating the mean transverse momentum component per nucleon in the reaction plane in a hemisphere, or as a function of rapidity, see Figs 4 and 5.

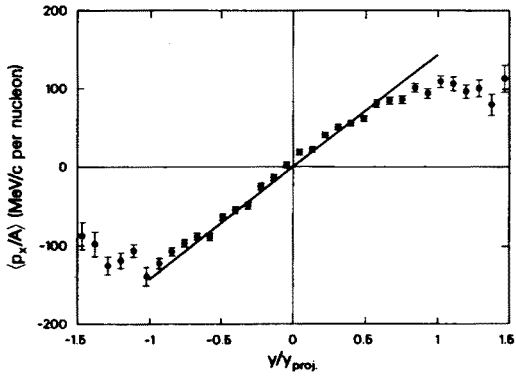

Fig. 5. Mean transverse momentum per nucleon projected onto reaction plane as a function of the normalized center of mass rapidity for Nb + Nb reaction at 400 MeV/nucleon [14].

When data on sideward deflection were compared to the results of transport-model calculations utilizing a density-dependent potential $V = V(n)$, *cf.* (5), a high value of compressibility $K = 380$ MeV was deduced [15]. However, after a momentum-dependence of the potential, known from the nucleon-nucleus scattering, was introduced [16], it became clear that data could also accommodate a low compressibility, *e.g.* $K = 215$ MeV. In a recent work with Pan [17], we found that existing data on sideward flow, with good [18] and poor [19] detection efficiency around beam axis, permit a separate assessment of the effects of momentum-dependence and density-dependence of the potential in the collisions, allowing to narrow the value of K.

In comparisons to data we have used the value of the slope of the mean momentum per mass at midrapidity [14, 19], *cf.* Fig. 5,

$$F = \left. \frac{d < p^x/m >}{dy} \right|_{y_0}, \tag{11}$$

in order to avoid the uncertainties associated with fragmentation. Further, the emitted particles in the model were subjected to the detector-acceptance filters. Fig. 6 shows that Plastic Ball data [18] may be described equally well by using a potential that corresponds to a low value of K and has a strong momentum-dependence, as by using a potential that corresponds to a high value of K. However, the DIOGENE data [19] can only be described using a potential with a strong momentum-dependence. This paradox may be resolved by examining Fig. 7, and considering the detector acceptance. In the figure we show the values of average cosine with respect to the reaction plane, as a function of transverse momentum, of the particles emitted in the

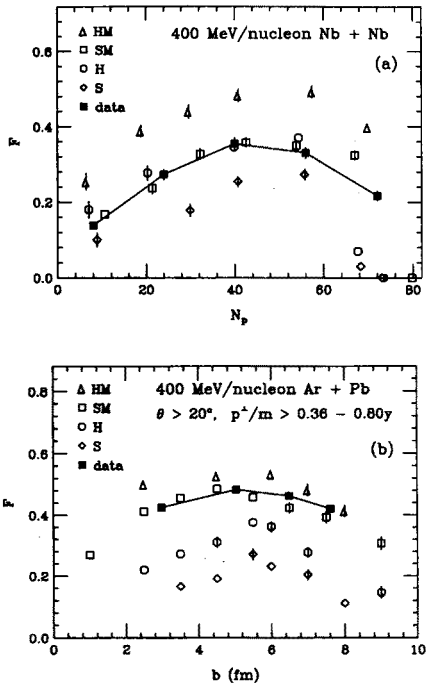

Fig. 6. Flow parameter F in Nb+Nb (a) and Ar+Pb (b) reactions at 400 MeV per nucleon. Data of Refs [18, 19] (filled squares) are compared to the results of calculations [17] for different optical potentials (open symbols). In (a) and (b) the abscissa shows participant proton multiplicity and impact parameter respectively.

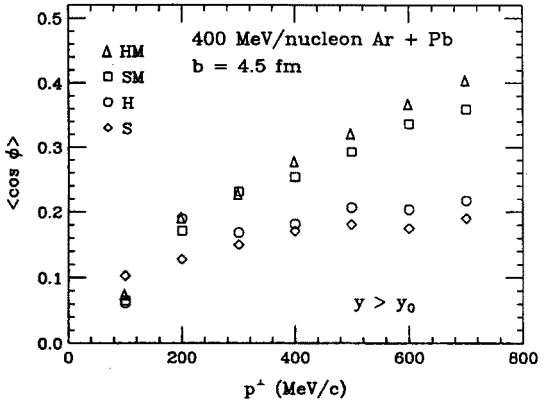

Fig. 7. Mean cosine of the azimuthal angle with respect to the reaction plane, of nucleons emitted at $y > y_0$, as a function of the nucleon transverse momentum.

forward rapidity region, for different potentials. It is seen that a momentum-dependent potential focuses more the high-momentum particles in the vicinity of the reaction plane than does a momentum-independent potential. The DIOGENE detector setup has a poor acceptance for particles emitted with low $p^{\perp}$, in contrast to the Plastic Ball setup. The acceptance enhances the flow values for the potentials with a strong momentum-dependence relative to potentials that lack that dependence.

By varying parameters in the calculation we managed [17] to put limits on compressibility: 165 MeV $< K <$ 220 MeV.

7. Light cluster production

Interest in the light-cluster production has been recently rather limited. This was due, in part, to the belief that the light-cluster spectra behave as powers of the nucleon spectrum,

$$\frac{d^3N_x}{dp_x^3} \propto \left(\frac{d^3N_N}{d(p_x/A)^3}\right)^A, \tag{12}$$

and thus contain no dynamic information beyond that in the nucleon spectrum. Recently, a dynamic model of light-cluster production was proposed [20, 21], with the cluster phase-space distribution functions satisfying Boltzmann equations similar to that satisfied by the nucleon function. Cluster spectra were found within the model to be useful for assessing the energy of collective expansion in the reactions.

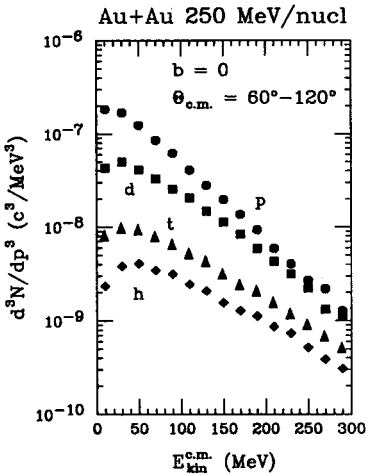

Fig. 8. Spectra of protons (filled circles), deuterons (squares), tritons (triangles), and helions (diamonds) from the $b = 0$, Au + Au reaction at 250 MeV/nucleon, in the range of the c.m. polar angle θ between 60° and 120°, after [21].

In the model [20, 21] the $A \leq 3$ clusters are produced in few-nucleon collisions involving a spectator and the constituent nucleons. The processes are related by time reversal to cluster break-up. The model reproduces [20, 22] the measured yields in the minimum-bias [4] and multiplicity-selected events [13] and further the spectra from the minimum-bias events, exhibiting the scaling (12). The latter events are dominated by those that are peripheral.

Fig. 8 shows the spectrum of particles from the simulation of a $b = 0$, Au + Au reaction at 250 MeV/nucleon, in the vicinity of 90° in the center of mass. Violation of the relation (12) is observed. With the proton spectrum being approximately exponential in the c.m. energy, the cluster spectra should be exponential, following (12), with the same slope as the nucleon spectrum. Analysis within the model [21] shows that a collective flow with local equilibrium is established in the collision prior to the freezeout, and

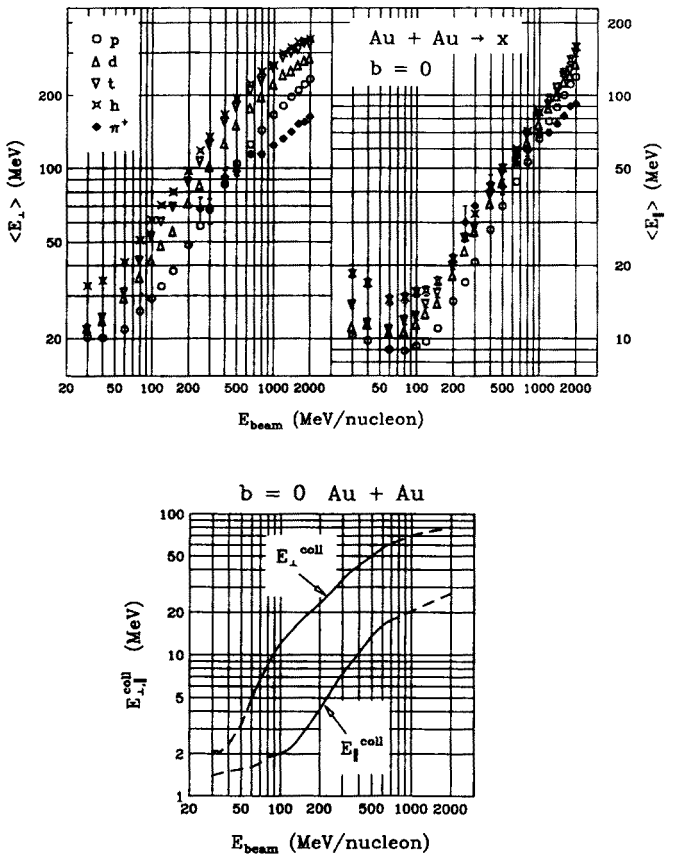

Fig. 9. Mean particle energies and collective energies at freezeout decomposed into longitudinal and transverse components in the $b = 0$, Au + Au collisions, as a function of bombarding energy.

affects the spectra.

In case of an instantaneous freezeout at a constant density and temperature, with the collective expansion present, the mean particle energies would rise linearly with mass,

$$\langle E\rangle = \frac{m\langle v^2\rangle}{2} + \frac{3}{2}T = A\frac{m_N\langle v^2\rangle}{2} + \frac{3}{2}T = AE_N^{\rm coll} + \frac{3}{2}T\,. \qquad (13)$$

The mean-energy differences could then be used to assess the nucleon collective energy. (Note that in case of (12) with an exponential proton spectrum the mean energies should stay constant with the mass). Fig. 9 shows the mean fragment energies decomposed into the longitudinal and transverse components in the reactions at $b = 0$, as a function of bombarding energy, and further the collective energy estimated at freezeout decomposed into the components. Energies of fragments with different mass are different, and particularly deuteron–proton energy-differences follow rather closely the collective energy. The theoretical investigation of the light-fragment spectra in central collisions parallels an experimental investigation of the spectra of the intermediate-mass fragments [23]. The calculated energies [21] partially agree and partially disagree with the Plastic Ball results [24] for the light fragments. An experimental reexamination of these energies will soon follow [25].

8. Conclusion

Let me conclude with an outlook at areas of research in the near future. From those discussed, the phenomenon of collective expansion is very likely to undergo scrutiny, with its importance recognized from low to ultrarelativistic energies. This phenomenon is tied to the entropy production, and further affects correlations and meson yields. The recent results on compressibility, utilizing sideward flow require a confirmation within other models with different parametrizations of the average potential. Change of the alignment with the reaction plane with the change of a transverse momentum awaits a direct experimental investigation.

From the phenomena little or not discussed, the fragmentation in collisions is not well understood. The production of pions with a long de Broglie's wavelength, together with the propagation of off-shell Δ resonances, may stick well outside of the domain of a semiclassical transport theory of collisions. A peak observed in the pion spectrum at low transverse momentum awaits an explanation. Production of other mesons and of the antibaryons and effects of the medium on those particles are of a wide interest.

REFERENCES

[1] H. Heiselberg, C.J. Pethick, D.G. Ravenhall, *Phys. Rev. Lett.* **61**, 818 (1988).
[2] Y. Yariv, Z. Frankel, *Phys. Rev.* **C20**, 2227 (1979).
[3] J. Cugnon, *Phys. Rev.* **C22**, 1885 (1980).
[4] S. Nagamiya *et al.*, *Phys. Rev.* **C24**, 971 (1981).
[5] B.V. Jacak *et al.*, *Phys. Rev. Lett.* **51**, 1846 (1984).
[6] H. Kruse *et al.*, *Phys. Rev.* **C31**, 1770 (1985).
[7] G.F. Bertsch, S. Das Gupta, H. Kruse, *Phys. Rev.* **C29**, 673 (1984).
[8] G.F. Bertsch, S. Das Gupta, *Phys. Rep.* **160**, 189 (1988).
[9] S.E. Koonin, *Phys. Lett.* **B70**, 43 (1977).
[10] W.G. Gong *et al.*, *Phys. Rev.* **C43**, 1804 (1991).
[11] J.J. Molitoris, H. Stöcker, B.L. Winer, *Phys. Rev.* **C36**, 220 (1987).
[12] P.J. Siemens, J.I. Kapusta, *Phys. Rev. Lett.* **43**, 1690 (1979); G. Bertsch, J. Cugnon, *Phys. Rev.* **C24**, 2514 (1981).
[13] K.G.R. Doss *et al.*, *Phys. Rev.* **C32**, 116 (1985).
[14] K.G.R. Doss *et al.*, *Phys. Rev. Lett.* **57**, 302 (1986).
[15] J.J. Molitoris, H. Stöcker, *Phys. Rev.* **C32**, 346 (1985).
[16] C. Gale *et al.*, *Phys. Rev.***C35**, 1666 (1987); J. Aichelin *et al.*, *Phys. Rev. Lett.* **58**, 1926 (1987).
[17] Q. Pan, P. Danielewicz, *Phys. Rev. Lett.* **70**, 2062, 3523 (1993).
[18] H. Å. Gustafsson *et al.*, *Mod. Phys. Lett.* **A3**, 1323 (1988).
[19] M. Demoulins, Ph. D. Thesis, University Paris Sud, 1989 [CEN Saclay Report No. CEA-N-2628, 1990]; J. Gosset, *et al.*, in *The Nuclear Equation of State,* eds W. Greiner and H. Stöcker, *NATO ASI Ser. A* **216**, Plenum, New York, 1989, p. 87.
[20] P. Danielewicz, G.F. Bertsch, *Nucl. Phys.* **A533**, 712 (1991).
[21] P. Danielewicz, Q. Pan, *Phys. Rev.* **C46**, 2002 (1992).
[22] P. Danielewicz, *Nucl. Phys.* **A545**, 21c (1992).
[23] S.C. Jeong *et al.*, Gesellschaft für Schwerionenforschung Report GSI-93-38, 1993.
[24] K.G.R. Doss *et al.*, *Mod. Phys. Lett.* **A3**, 849 (1988).
[25] G. Poggi, private communication.